Available online at www.sciencedirect.com
ScienceDirect
International Journal of Heat and Mass Transfer 51 (2008) 1920–1932
International Journal of HEAT and MASS TRANSFER
www.elsevier.com/locate/ijhmt

Estimation of heat-transfer characteristics on a vertical annular circular fin of finned-tube heat exchangers in forced convection

Han-Taw Chen *, Wei-Lun Hsu

Department of Mechanical Engineering, National Cheng Kung University, Tainan 701, Taiwan

Received 19 January 2007; received in revised form 17 June 2007
Available online 6 September 2007

Abstract

The finite difference method in conjunction with the least-squares scheme and experimental measured temperatures is applied to predict the average heat transfer coefficient $\bar{h}$ and fin efficiency η_f on a vertical annular circular fin of finned-tube heat exchangers for various fin spacings in forced convection. The distribution of the heat transfer coefficient on the fin is assumed to be non-uniform, thus the whole annular circular fin is divided into several sub-fin regions in order to predict the $\bar{h}$ and η_f values. These two predicted values can be obtained using the present inverse scheme in conjunction with the experimental measured temperatures. The results show that the effect of the fin spacing S on the $\bar{h}$ value can be negligible when the S value exceeds about 0.018 m. The $\bar{h}$ value increases with increasing the air speed V_{air} for 1 m/s $\leqslant V_{air} \leqslant$ 5 m/s ($1550 \leqslant Re_d \leqslant 7760$) and increasing the fin spacing for 0.005 m $\leqslant S \leqslant$ 0.018 m. The present estimated results can be applied to obtain the new correlations of the Nusselt number and fin efficiency based on d_o, S and Re_d. The average heat transfer coefficients obtained from this new correlation of the Nusselt number are in good agreement with those given by Hu and Jacobi [X. Hu, A.M. Jacobi, Local heat transfer behavior and its impact on a single-row, annularly finned tube heat exchanger, ASME J. Heat Transfer 115 (1993) 66–74].

1. Introduction

Annular-finned tube heat exchangers are commonly used in industry. In designing such heat exchangers, it is necessary to note the interactions between the local heat transfer and flow distribution within the fins. The previous works about the effect of the fin spacing of annular-finned tube heat exchangers were limited to the experiments [1]. Thus the present study applies the hybrid inverse scheme in conjunction with experimental temperature data to estimate the heat-transfer characteristics of annular-finned tube heat exchangers in forced convection. The fin in heat exchangers is always applied to increase the heat flow per unit of basic surface. The analysis of a continuous plate fin pierced by a regularly spaced array of circular tubes in staggered and in-line arrays has many engineering applications [2]. In order to simplify the problem considered, the calculation of the standard fin efficiency usually assumed that the heat transfer coefficient was constant over the plate fin. It can be found from Refs. [3–6] that there exhibited very complex three-dimensional flow characteristics within a plate finned-tube heat exchanger. In particular, complex flow patterns caused by the horseshoe vortices at the corner junction are of interest to the study of local heat transfer enhancement mechanism. The flow accelerates around a heated horizontal annular-finned circular tube in a cross-flow and forms a low-velocity wake region behind the tube. The boundary layer over a heated horizontal tube starts to develop at the front of the tube and increases in thickness along the circumference of the tube. Thus the heat transfer coefficient in forced convection is highest on the upstream fin region and is lowest on the wake fin region, as shown in Ref. [7]. This causes local variations of the heat transfer coefficient on the fin. On the other hand, the heat transfer coefficient on the fin is non-uniform. As shown in Ref. [8],

* Corresponding author. Fax: +886 6 2352973.
E-mail address: htchen@mail.ncku.edu.tw (H.-T. Chen).

0017-9310/$ - see front matter © 2007 Elsevier Ltd. All rights reserved.
doi:10.1016/j.ijheatmasstransfer.2007.06.035

Nomenclature

A_f	area of the annular circular fin, m^2
A_j	area of the jth sub-fin region, m^2
$[A]$	global conduction matrix
D_H	hydraulic diameter of heat exchanger, m
d_o	outer diameter of the circular tube, m
$[F]$	force matrix
g	acceleration of gravity, m/s^2
h	local heat transfer coefficient, W/m^2 K
$\bar{h}$	unknown average heat transfer coefficient, W/m^2 K
$\bar{h}^{iso}$	unknown average heat transfer coefficient under the isothermal condition, W/m^2 K
h_f	fin height, $R_o - R_i$
$\bar{h}_j$	unknown average heat transfer coefficient on the jth sub-fin region, W/m^2 K
k_f	thermal conductivity of the fin, W/m K
k_{air}	thermal conductivity of the air, W/m K
ℓ_r	distance between two neighboring nodes in the r-direction, $\ell_r = (R_o - R_i)/(N_r - 1)$
ℓ_θ	distance between two neighboring nodes in the θ-direction, $\ell_\theta = 2\pi/(N_\theta - 1)$
N	number of sub-fin regions
Nu_d^{iso}	Nusselt number defined in Eq. (22)
N_r	number of nodes in the r-direction
N_θ	number of nodes in the θ-direction
Q	total heat transfer rate dissipated from the annular circular fin, W
q_j	heat transfer rate dissipated from the jth sub-fin region, W
r	spatial coordinate
R_i	inner radius of the annular circular fin or outer radius of the circular tube, m
R_o	outer radius of the annular circular fin, m
Re	Reynolds number defined in Eq. (23)
Re_d	Reynolds number defined in Eq. (24)
S	fin spacing, m
T	fin temperature, K
T_f	film temperature, $(T_o + T_\infty)/2$
T_j	measured temperature on the jth sub-fin region, K
T_o	outer surface temperature of the circular tube, K
T_∞	ambient temperature, K
$[T]$	global temperature matrix
V_{air}	frontal air speed, m/s
V_{max}	maximum air speed, m/s

Greek symbols

α	thermal diffusivity of the air, m^2/s
β	volumetric thermal expansion coefficient, 1/K
δ	fin thickness, m
η_f	fin efficiency
ν	kinematic viscosity of the air, m^2/s
θ	spatial coordinate

Superscripts

cal	calculated value
mea	measured data

the measurement of the local heat transfer coefficient on the plate fin under steady-state heat transfer conditions was very difficult to perform, since the local fin temperature and local heat flux were required. Moreover, reliability is an important concept in engineering design, and the use of reliable components enables the designers to utilize more sophisticated techniques to improve the performance [9]. Thus the estimation of a more accurate heat transfer coefficient on the fin is an important task for the device of the high-performance heat exchangers.

Heat transfer coefficients encountered in forced convection are typically much higher than those encountered in natural convection because of the higher fluid velocities associated with forced convection. As a result, most of researchers tend to ignore natural convection in heat transfer analyses that involve forced convection. However, this error may be considerable at low velocities associated with forced convection [10].

It is known that the physical quantities of the test material can be predicted using the measured temperatures inside this test material. Such problems are called the inverse heat conduction problems that have become an interesting subject recently. To date, various inverse methods in conjunction with the measured temperatures inside the test material have been developed for the analysis of the inverse heat conduction problems [11,12]. However, to the authors' knowledge, a few researchers performed the prediction of the local heat transfer coefficients on a vertical annular circular fin of finned-tube heat exchangers with regard for the effect of the fin spacing [3–7,13,15–17].

Sung et al. [3] applied the naphthalene sublimation technique to obtain the local mass transfer coefficient on a circular cylinder with transverse two annular fins in a cross flow. Hu and Jacobi [6] also applied the naphthalene sublimation technique to obtain the local convective heat and mass transfer coefficients on a circular cylinder with transverse annular fins in a cross flow over the Reynolds number ranging from 3300 to 12,000. Watel et al. [14] investigated the influence of the flow velocity and fin spacing on the forced convective heat transfer from a single annular-finned tube using the Particle Image Velocimetry and infrared thermography. They obtained a valuable correlation of the mean Nusselt number on the fin as a function of the dimensionless fin spacing, outer diameter of a circular tube

and Reynolds number for $2550 \leqslant Re_d \leqslant 42{,}000$. They also found that the reduction in fin spacing leaded to a decrease of heat transfer for a fixed Reynolds number. However, the difference of the average heat transfer coefficients on the downstream and upstream fin regions and fin efficiency was not shown in Ref. [14]. As stated by Hu and Jacobi [6], it was difficult to obtain fin efficiency measurements, because the temperature measurements within the fin or on its surface are inherently difficult to make without disrupting the heat transfer behavior. Mon and Gross [15] applied the three-dimensional numerical study to investigate the effect of the fin spacing on four-row annular-finned tube bundles in staggered and in-line arrangements. The heat transfer and fluid flow characteristics were predicted using the computational fluid dynamics commercial code of FLUENT. It can be found from Ref. [15] that the laminar flow between the fins and one-dimensional heat conduction equation were assumed. Sparrow and Samie [16] measured Nusselt numbers and pressure loss coefficients for one- and two-row arrays of annular-finned tubes using the experimental method. Matos et al. [17] applied a theoretical, numerical and experimental study to demonstrate that finned and non-finned circular and elliptic tubes heat exchangers in forced convection that can be optimized for maximum heat transfer under a fixed volume constraint. Jang [18] used the numerical and experimental studies to estimate the heat transfer and fluid flow characteristics of a four-row annular-finned tube heat exchanger in a staggered arrangement in order to develop the high efficiency air-cooled steam condenser for the power plant. Sometimes, it is maybe difficult to measure the temperature distributions on the fin of plate finned-tube heat exchangers using the infrared thermography and thermocouples for some practical heat transfer problems. Due to this reason, Chen and Hsu [13] applied the finite difference method in conjunction with the least-squares scheme and experimental measured temperatures to predict the natural-convection heat transfer coefficient and fin efficiency on a vertical annular circular fin of finned-tube heat exchangers in a small open box with regard for the effect of the fin spacing. It can be found that the predicted results of the average heat transfer coefficient given in Ref. [13] agreed with those obtained from the correlations recommended by current textbooks [1,19] under the assumption of the ideal isothermal fin. This implies that the present inverse scheme has good reliability. In order to validate the reliability and accuracy of the present inverse scheme in forced convection further, the present study performs the estimations of the average heat transfer coefficient and fin efficiency on a vertical annular circular fin of finned-tube heat exchangers in forced convection. The present estimated results of the average heat transfer coefficient under the ideal isothermal condition will compare with the estimated results given by Hu and Jacobi [6] and Watel et al. [14].

The inverse analysis of the present study is that the whole fin area is divided into several analysis sub-fin regions and then the fin temperatures at selected measurement locations are measured using T-type thermocouples. Later, the finite difference method in conjunction with the measured temperatures and least-squares method is applied to predict the average heat transfer coefficients on these sub-fin regions. Furthermore, the average heat transfer coefficient $\bar{h}$ and fin efficiency can be obtained for various air speeds and fin spacings under the given conditions of the ambient and tube temperatures. The computational procedures for the estimates of the heat transfer coefficient on each sub-fin region are performed repeatedly until the sum of the squares of the deviations between the calculated and measured temperatures becomes minimum.

2. Mathematical formulation

The schematic diagram of the present problem is shown in Fig. 1. Fig. 2 shows the physical model of the two-dimensional thin annular circular fin with measurement locations and sub-fin regions in forced convection. R_o and R_i denote the outer and inner radii of the annular circular fin, respectively. S and δ, respectively, denote the fin spacing and fin thickness. The center of the circular tube is located at $r = 0$. T_o and T_∞, respectively, denote the outer surface temperature of the circular tube and the ambient temperature. Due to the thin fin behavior, the temperature gradient in the z-direction (the fin thickness) is small and the fin temperature varies only in the r- and θ-directions. The "insulated tip" assumption can be an adequate approximation provided that the actual heat transfer rate dissipated through the tip is much smaller than the total heat transfer rate drawn from the base wall [20]. It can be found from Refs. [7,13] that the heat transfer coefficient on the fin of finned-tube heat exchangers was non-uniform. Thus the heat transfer coefficient $h(r,\theta)$ in the present study is also assumed to be non-uniform. The average heat trans-

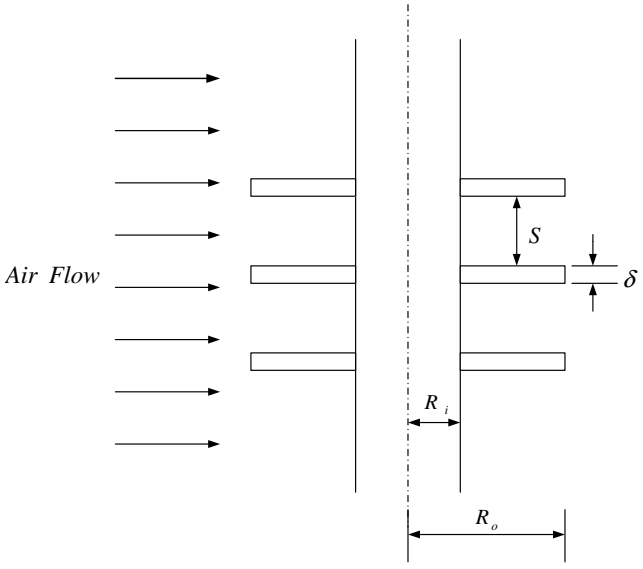

Fig. 1. Schematic diagram of one-tube annular-finned tube heat exchangers in forced convection.

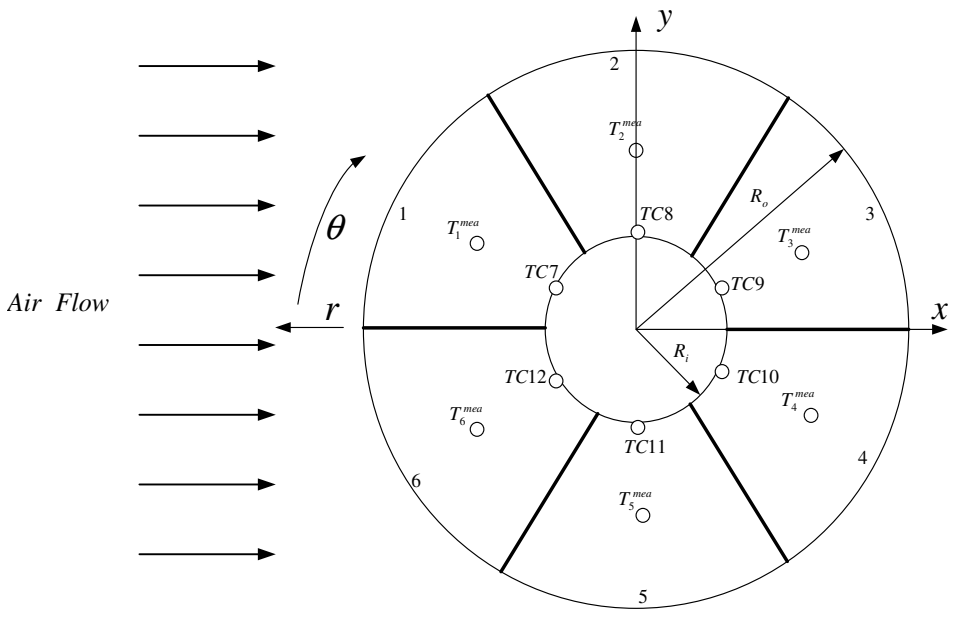

Fig. 2. Physical model of a two-dimensional annular circular fin with measurement locations and sub-fin regions in forced convection.

fer coefficient on each sub-fin region can be estimated provided that the fin temperatures at various measurement locations can be measured. Under the assumptions of the steady state and constant thermal properties, the two-dimensional heat conduction equation for the continuous the fin of a one-tube finned-tube heat exchanger can be expressed as

$$\frac{\partial^2 T}{\partial r^2}+\frac{1}{r}\frac{\partial T}{\partial r}+\frac{1}{r^2}\frac{\partial^2 T}{\partial \theta^2}=\frac{2h(r,\theta)}{k_{\mathrm{f}}\delta}(T-T_\infty)\ \text{in}\ R_i<r<R_{\mathrm{o}},\ 0<\theta\leqslant 2\pi \tag{1}$$

Its corresponding boundary conditions are

$$\frac{\partial T(r,0)}{\partial \theta}=\frac{\partial T(r,2\pi)}{\partial \theta} \tag{2}$$

$$T(r,0)=T(r,2\pi) \tag{3}$$

$$T(r,\theta)=T_{\mathrm{o}}\quad \text{at}\ r=R_i \tag{4}$$

and

$$\frac{\partial T(r,\theta)}{\partial r}=0\quad \text{at}\ r=R_{\mathrm{o}} \tag{5}$$

where T is the fin temperature. r and θ are cylindrical coordinates. $h(r,\theta)$ is the unknown heat transfer coefficient on the fin. k_{f} is the thermal conductivity of the fin.

3. Numerical analysis

It might be difficult to measure the temperature distributions on the annular circular fin using the infrared thermography and thermocouples for some practical heat transfer problems. Relatively, the distribution of the unknown heat transfer coefficient on a fin $h(r,\theta)$ is not easy to be obtained. Under this circumstance, the annular circular fin considered can be divided into N sub-fin regions in the present inverse scheme and then the unknown heat transfer coefficient on each sub-fin region can be assumed to be constant. Thus the application of the finite difference method to Eq. (1) can produce the following difference equation on the kth sub-fin region as

$$\begin{aligned}&\frac{T_{i+1,j}-2T_{i,j}+T_{i-1,j}}{\ell_r^2}+\frac{1}{R_i+(i-1)\ell_r}\frac{T_{i+1,j}-T_{i-1,j}}{2\ell_r}\\&+\frac{1}{[R_i+(i-1)\ell_r]^2}\frac{T_{i,j+1}-2T_{i,j}+T_{i,j-1}}{\ell_\theta^2}\\&=\frac{2\bar{h}_k}{k_{\mathrm{f}}\delta}(T_{i,j}-T_\infty)\\&\text{for}\ i=2,\ldots,N_r,\\&j=(N_\theta-1)(k-1)/N+2,(N_\theta-1)(k-1)/N+3,\ldots,\\&(N_\theta-1)k/N\end{aligned} \tag{6}$$

where ℓ_r and ℓ_θ, respectively, are the distances between two neighboring nodes in the r- and θ-directions and are defined as $\ell_r=(R_{\mathrm{o}}-R_{\mathrm{i}})/(N_r-1)$ and $\ell_\theta=2\pi/(N_\theta-1)$. N_r and N_θ are the nodal numbers in the r- and θ-directions, respectively. $\bar{h}_k$ is denoted as the average heat transfer coefficient on the kth sub-fin region.

The application of the central difference approximation to the boundary condition (2) and then the substitution of the resulting equation into Eq. (6) can yield the difference equations as

$$\begin{aligned}&\frac{T_{i+1,1}-2T_{i,1}+T_{i-1,1}}{\ell_r^2}+\frac{1}{R_i+(i-1)\ell_r}\frac{T_{i+1,1}-T_{i-1,1}}{2\ell_r}\\&+\frac{1}{[R_i+(i-1)\ell_r]^2}\frac{T_{i,2}-2T_{i,1}+T_{i,N_\theta-1}}{\ell_\theta^2}\\&=\frac{2\bar{h}_m}{k_{\mathrm{f}}\delta}(T_{i,1}-T_\infty)\quad \text{for}\ i=2,3,\ldots,N_r\end{aligned} \tag{7}$$

and

$$\frac{T_{i+1,N_\theta}-2T_{i,N_\theta}+T_{i-1,N_\theta}}{\ell_r^2}+\frac{1}{R_i+(i-1)\ell_r}\frac{T_{i+1,N_\theta}-T_{i-1,N_\theta}}{2\ell_r}+\frac{1}{[R_i+(i-1)\ell_r]^2}\frac{T_{i,2}-2T_{i,N_\theta}+T_{i,N_\theta-1}}{\ell_\theta^2}=\frac{2\bar{h}_m}{k_f\delta}(T_{i,N_\theta}-T_\infty)\quad \text{for } i=2,3,\ldots,N_r \tag{8}$$

where $\bar{h}_m$ is defined as $\bar{h}_m=(\bar{h}_1+\bar{h}_N)/2$.

The discretized form of Eq. (4) is given as

$$T_{1,j}=T_o\quad \text{for } j=1,2,\ldots,N_\theta \tag{9}$$

The application of the central difference approximation to the boundary conditions (3) and (5) can yield their difference equations as

$$T_{i,1}=T_{i,N_\theta}\quad \text{for } i=2,3,\ldots,N_r \tag{10}$$

and

$$T_{N_r-1,j}=T_{N_r+1,j}\quad \text{for } j=1,2,\ldots,N_\theta \tag{11}$$

The difference equations for the nodes at the interface of two neighboring sub-fin regions, as shown in Fig. 3, can be expressed as

$$\frac{T_{i+1,j}-2T_{i,j}+T_{i-1,j}}{\ell_r^2}+\frac{1}{R_i+(i-1)\ell_r}\frac{T_{i+1,j}-T_{i-1,j}}{2\ell_r}+\frac{1}{[R_i+(i-1)\ell_r]^2}\frac{T_{i,j+1}-2T_{i,j}+T_{i,j-1}}{\ell_\theta^2}=\frac{\bar{h}_k+\bar{h}_{k+1}}{k_f\delta}(T_{i,j}-T_\infty)$$
$$\text{for } i=2,\ldots,N_r,\ \ j=(N_\theta-1)k/N+1,\quad k=1,2,\ldots,N-1 \tag{12}$$

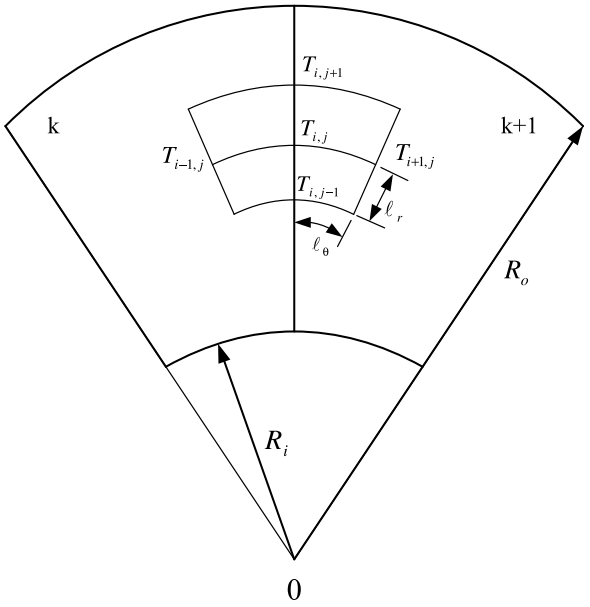

Fig. 3. Nodes at the interface of two-neighboring sub-fin areas.

Rearrangement of Eqs. (6)–(12) can yield the following matrix equation as

$$[A][T]=[F] \tag{13}$$

where $[A]$ is a global conduction matrix. $[T]$ is a matrix representing the nodal temperatures. $[F]$ is a force matrix. The nodal temperatures can be obtained from Eq. (13) using the Gauss elimination algorithm.

Once the average heat transfer coefficient on each sub-fin region is obtained, the heat transfer rate dissipated from the jth sub-fin region q_i and average heat transfer coefficient on the whole fin $\bar{h}$ can be determined using the following expressions. The heat transfer rate dissipated from the jth sub-fin region q_i is defined as

$$q_i=2\bar{h}_j\int_{A_j}(T-T_\infty)\mathrm{d}A\quad \text{for } j=1,2,\ldots,N \tag{14}$$

The average heat transfer coefficient on the whole fin $\bar{h}$ can be expressed as

$$\bar{h}=\sum_{j=1}^{N}\bar{h}_jA_j/A_f \tag{15}$$

where A_f is the area of the annular circular fin. A_j is the area of the jth sub-fin region.

The fin efficiency η_f is defined as the ratio of the actual heat transfer rate from the whole fin to the dissipated heat transfer rate from the fin maintained at the tube temperature T_o. Thus the fin efficiency η_f can be expressed as

$$\eta_f=\frac{\sum_{j=1}^{N}q_j}{2A_f(T_o-T_\infty)\bar{h}} \tag{16}$$

The total heat transfer rate dissipated from the whole fin to the ambient Q can be written as

$$Q=\sum_{j=1}^{N}q_j \tag{17}$$

In order to estimate the unknown heat transfer coefficient on the jth sub-fin region $\bar{h}_j$, the additional information of the steady-state measured temperatures is required. The more a number of the sub-fin regions are, the more accurate the estimation of the unknown average heat transfer coefficient on the whole fin can be. Relatively, a more computational time can be required. In the present study, T-type thermocouples are used to record the temperature information at selected measurement locations. The measured temperature taken from the jth thermocouple is denoted as T_j^{mea}, $j=1,\ldots,N$, as shown in Tables 1–3.

The least-squares minimization technique is applied to minimize the sum of the squares of the deviations between the calculated and measured temperatures at selected measurement locations. In the present study, the unknown average heat transfer coefficients on each sub-fin region $\bar{h}_i$ can be expressed as

$$\bar{h}_i=C_i\quad \text{for } i=1,2,\ldots,N \tag{18}$$

Table 1
Temperature measurements and the present estimates for $V_{air} = 1$ m/s and various S values

		$S = 0.005$ m $T_0 = 330.63$ K $T_\infty = 298.03$ K	$S = 0.01$ m $T_0 = 328.82$ K $T_\infty = 298.20$ K	$S = 0.015$ m $T_0 = 330.34$ K $T_\infty = 299.74$ K	$S \to \infty$ $T_0 = 335.03$ K $T_\infty = 300.23$ K
T_j^{mea} (K)		$T_1^{mea} = 305.67$ $T_2^{mea} = 305.83$ $T_3^{mea} = 314.30$ $T_4^{mea} = 312.93$ $T_5^{mea} = 305.91$ $T_6^{mea} = 303.70$	$T_1^{mea} = 304.71$ $T_2^{mea} = 305.36$ $T_3^{mea} = 309.22$ $T_4^{mea} = 309.28$ $T_5^{mea} = 305.39$ $T_6^{mea} = 303.17$	$T_1^{mea} = 305.51$ $T_2^{mea} = 305.67$ $T_3^{mea} = 313.25$ $T_4^{mea} = 311.31$ $T_5^{mea} = 307.67$ $T_6^{mea} = 304.75$	$T_1^{mea} = 306.67$ $T_2^{mea} = 307.06$ $T_3^{mea} = 312.75$ $T_4^{mea} = 312.75$ $T_5^{mea} = 309.22$ $T_6^{mea} = 306.16$
$\bar{h}_j$ (W/m^2 K)		$\bar{h}_1 = 24.72$ $\bar{h}_2 = 35.86$ $\bar{h}_3 = 3.20$ $\bar{h}_4 = 7.49$ $\bar{h}_5 = 31.02$ $\bar{h}_6 = 45.46$	$\bar{h}_1 = 29.65$ $\bar{h}_2 = 31.97$ $\bar{h}_3 = 12.51$ $\bar{h}_4 = 12.51$ $\bar{h}_5 = 29.40$ $\bar{h}_6 = 48.96$	$\bar{h}_1 = 34.35$ $\bar{h}_2 = 45.10$ $\bar{h}_3 = 4.06$ $\bar{h}_4 = 13.98$ $\bar{h}_5 = 24.56$ $\bar{h}_6 = 48.50$	$\bar{h}_1 = 36.27$ $\bar{h}_2 = 41.00$ $\bar{h}_3 = 11.20$ $\bar{h}_4 = 13.62$ $\bar{h}_5 = 24.74$ $\bar{h}_6 = 45.60$
q_j (W)		$q_1 = 0.72$ $q_2 = 1.11$ $q_3 = 0.14$ $q_4 = 0.32$ $q_5 = 0.95$ $q_6 = 1.11$	$q_1 = 0.77$ $q_2 = 0.90$ $q_3 = 0.43$ $q_4 = 0.43$ $q_5 = 0.82$ $q_6 = 1.09$	$q_1 = 0.85$ $q_2 = 1.19$ $q_3 = 0.16$ $q_4 = 0.51$ $q_5 = 0.72$ $q_6 = 1.08$	$q_1 = 1.01$ $q_2 = 1.22$ $q_3 = 0.44$ $q_4 = 0.54$ $q_5 = 0.82$ $q_6 = 1.17$
$\bar{h}$ (W/(m^{2}K))		24.63	27.50	28.42	28.74
$\bar{h}^{iso}$ W/(m^{2}K)	Present Eq. (20)	18.73	20.35	20.69	20.97
	Present Eq. (25)	18.49	19.37	19.55	21.02
	Ref. [14]	18.49	21.04	21.98	25.73
Q (W)		4.35	4.44	4.51	5.20
η_f		38%	37%	36%	35%

Table 2
Temperature measurements and the present estimates for $V_{air} = 3$ m/s and various S values

		$S = 0.005$ m $T_0 = 331.70$ K $T_\infty = 298.15$ K	$S = 0.01$ m $T_0 = 331.00$ K $T_\infty = 299.00$ K	S=0.015 m $T_0 = 330.80$ K $T_\infty = 299.90$ K	$S \to \infty$ $T_0 = 331.60$ K $T_\infty = 300.15$ K
T_j^{mea} (K)		$T_1^{mea} = 300.31$ $T_2^{mea} = 303.73$ $T_3^{mea} = 310.39$ $T_4^{mea} = 308.82$ $T_5^{mea} = 302.16$ $T_6^{mea} = 301.31$	$T_1^{mea} = 302.46$ $T_2^{mea} = 302.75$ $T_3^{mea} = 306.36$ $T_4^{mea} = 306.92$ $T_5^{mea} = 302.79$ $T_6^{mea} = 301.21$	$T_1^{mea} = 302.49$ $T_2^{mea} = 302.95$ $T_3^{mea} = 307.21$ $T_4^{mea} = 306.95$ $T_5^{mea} = 303.41$ $T_6^{mea} = 302.46$	$T_1^{mea} = 302.95$ $T_2^{mea} = 303.08$ $T_3^{mea} = 306.79$ $T_4^{mea} = 307.05$ $T_5^{mea} = 303.80$ $T_6^{mea} = 302.79$
$\bar{h}_j$ (W/m^2 K)		$\bar{h}_1 = 116.86$ $\bar{h}_2 = 45.01$ $\bar{h}_3 = 9.38$ $\bar{h}_4 = 14.13$ $\bar{h}_5 = 69.25$ $\bar{h}_6 = 73.28$	$\bar{h}_1 = 62.67$ $\bar{h}_2 = 67.67$ $\bar{h}_3 = 25.12$ $\bar{h}_4 = 20.89$ $\bar{h}_5 = 64.38$ $\bar{h}_6 = 107.52$	$\bar{h}_1 = 84.40$ $\bar{h}_2 = 80.43$ $\bar{h}_3 = 21.83$ $\bar{h}_4 = 25.12$ $\bar{h}_5 = 67.88$ $\bar{h}_6 = 87.12$	$\bar{h}_1 = 78.63$ $\bar{h}_2 = 84.43$ $\bar{h}_3 = 27.02$ $\bar{h}_4 = 26.16$ $\bar{h}_5 = 65.85$ $\bar{h}_6 = 86.73$
q_j (W)		$q_1 = 2.24$ $q_2 = 1.17$ $q_3 = 0.35$ $q_4 = 0.49$ $q_5 = 1.62$ $q_6 = 1.39$	$q_1 = 1.29$ $q_2 = 1.48$ $q_3 = 0.71$ $q_4 = 0.60$ $q_5 = 1.40$ $q_6 = 1.82$	$q_1 = 1.56$ $q_2 = 1.61$ $q_3 = 0.59$ $q_4 = 0.68$ $q_5 = 1.41$ $q_6 = 1.48$	$q_1 = 1.50$ $q_2 = 1.69$ $q_3 = 0.71$ $q_4 = 0.70$ $q_5 = 1.40$ $q_6 = 1.51$
$\bar{h}$ (W/(m^2 K))		54.65	58.04	61.13	61.47
$\bar{h}^{iso}$ (W/(m^2 K))	Present Eq. (20)	30.37	32.02	33.29	33.51
	Present Eq. (25)	30.96	31.67	31.78	33.62
	Ref. [14]	35.43	39.38	40.90	47.10
Q (W)		7.26	7.30	7.33	7.51
η_f		28%	28%	27%	27%

Table 3
Temperature measurements and the present estimates for $V_{air} = 5$ m/s and various S values

		$S = 0.005$ m $T_0 = 330.13$ K $T_\infty = 298.90$ K	$S = 0.01$ m $T_0 = 331.20$ K $T_\infty = 299.25$ K	$S = 0.015$ m $T_0 = 329.30$ K $T_\infty = 299.53$ K	$S \to \infty$ $T_0 = 331.50$ K $T_\infty = 299.88$ K
T_j^{mea} (K)		$T_1^{mea} = 300.98$ $T_2^{mea} = 301.37$ $T_3^{mea} = 306.43$ $T_4^{mea} = 308.75$ $T_5^{mea} = 300.98$ $T_6^{mea} = 300.86$	$T_1^{mea} = 301.80$ $T_2^{mea} = 301.97$ $T_3^{mea} = 305.11$ $T_4^{mea} = 305.41$ $T_5^{mea} = 301.67$ $T_6^{mea} = 300.82$	$T_1^{mea} = 301.18$ $T_2^{mea} = 301.64$ $T_3^{mea} = 304.43$ $T_4^{mea} = 305.25$ $T_5^{mea} = 301.48$ $T_6^{mea} = 301.18$	$T_1^{mea} = 301.44$ $T_2^{mea} = 302.39$ $T_3^{mea} = 304.13$ $T_4^{mea} = 304.92$ $T_5^{mea} = 302.13$ $T_6^{mea} = 301.61$
$\bar{h}_j$ (W/(m^2 K))		$\bar{h}_1 = 102.50$ $\bar{h}_2 = 98.83$ $\bar{h}_3 = 24.03$ $\bar{h}_4 = 7.68$ $\bar{h}_5 = 121.35$ $\bar{h}_6 = 107.11$	$\bar{h}_1 = 83.83$ $\bar{h}_2 = 90.25$ $\bar{h}_3 = 33.43$ $\bar{h}_4 = 29.36$ $\bar{h}_5 = 98.33$ $\bar{h}_6 = 137.38$	$\bar{h}_1 = 120.11$ $\bar{h}_2 = 103.57$ $\bar{h}_3 = 39.21$ $\bar{h}_4 = 27.64$ $\bar{h}_5 = 114.14$ $\bar{h}_6 = 119.16$	$\bar{h}_1 = 134.30$ $\bar{h}_2 = 89.38$ $\bar{h}_3 = 51.64$ $\bar{h}_4 = 37.36$ $\bar{h}_5 = 103.20$ $\bar{h}_6 = 120.46$
q_j (W)		$q_1 = 1.79$ $q_2 = 1.87$ $q_3 = 0.68$ $q_4 = 0.24$ $q_5 = 2.24$ $q_6 = 1.67$	$q_1 = 1.56$ $q_2 = 1.77$ $q_3 = 0.84$ $q_4 = 0.75$ $q_5 = 1.86$ $q_6 = 2.10$	$q_1 = 1.91$ $q_2 = 1.79$ $q_3 = 0.88$ $q_4 = 0.65$ $q_5 = 1.95$ $q_6 = 1.72$	$q_1 = 2.22$ $q_2 = 1.67$ $q_3 = 1.14$ $q_4 = 0.87$ $q_5 = 1.89$ $q_6 = 1.84$
$\bar{h}$ (W/(m^2 K))		76.92	78.76	87.30	89.39
$\bar{h}^{iso}$ (W/(m^2 K))	Present Eq. (20)	38.15	39.01	41.96	42.74
	Present Eq. (25)	39.27	39.79	39.83	41.82
	Ref. [14]	47.20	52.67	54.58	62.44
Q (W)		8.49	8.88	8.90	9.63
η_f		25%	25%	24%	24%

The error in the estimates $E(C_1, C_2, \ldots, C_N)$ will be minimized in order to obtain the required estimates. $E(C_1, C_2, \ldots, C_N)$ is defined as

$$E(C_1, C_2, \ldots, C_N) = \sum_{j=1}^{N} [T_j^{cal} - T_j^{mea}]^2 \tag{19}$$

where T_j^{cal} denotes the calculated temperature taken from the jth thermocouple location and is obtained from Eq. (13).

The estimated values of C_j, $j = 1, 2, \ldots, N$, are determined until the value of $E(C_1, C_2, \ldots, C_N)$ is minimum. The detailed computational procedures for estimating the C_j values, $j = 1, 2, \ldots, N$, can be found in Refs. [7,13]. In order to avoid repetition, they are not shown in this paper. The computational procedures of the present study are repeated until the values of $\left|\frac{T_j^{mea} - T_j^{cal}}{T_j^{mea}}\right|$, $j = 1, 2, \ldots, N$, are less than 10^{-6}.

4. Experimental apparatus

An experimental configuration of the small wind tunnel used for the present problem is the same as Fig. 1 of Ref. [7]. The experimental procedures and manners have also been shown in Ref. [7]. In order to avoid repetition, they are not shown in this study. Fig. 4 shows the experimental configuration of the test annular fin vertically mounted on a circular tube in forced convection. The test annular circular fin with 27 mm in inner diameter, 99 mm in outer diameter and 1 mm in thickness are made of AISI 304 stainless material. It can be found from Ref. [21] that the thermal conductivity of AISI 304 stainless material is 14.9 W/m K. An anemometer installed at 300 mm in front of the airflow entering the test specimen is used to measure the frontal air velocity. The limit of its error is ±0.4% for the velocity ranging from 0.4 m/s to 30.0 m/s. The ambient and test fin temperatures are measured using T-type thermocouples. The limit of error of the T-type thermocouple is ±0.4% for 0 °C ⩽ T ⩽ 350 °C. Six thermocouples, TC7, TC8, TC9, TC10, TC11 and TC12, placed in the gap between the fin and the circular tube are fixed at π/6, π/2, 5π/6, 7π/6, 3π/2 and 11π/6 in angle, as shown in Fig. 2. In order to reduce the heat loss between the fin and the circular tube, their gap is filled with the cyanoacrylate (Satlon, D-3). The average of these six measured temperatures is taken as the fin base temperature and is also assumed to be the outer surface temperature of the circular tube T_0 in the present study. Three thermocouples penetrated the central line of the top surface and two lateral surfaces are positioned at 100 mm away from the test fin in order to measure the ambient temperature T_∞. The average of these three measured temperatures is taken as the ambient temperature T_∞. In order to estimate the average heat transfer coefficient on the fin, the annular circular fin

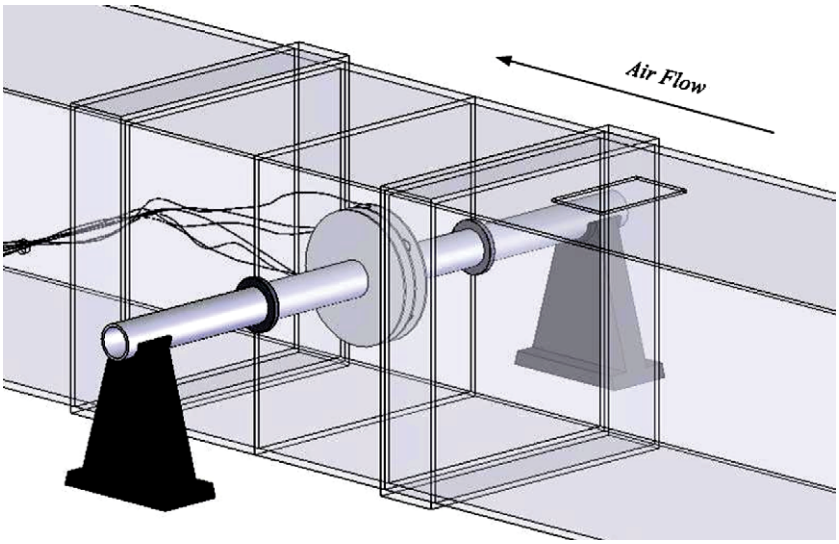

Fig. 4. Experimental configuration of the test annular fin vertically mounted on a circular tube in forced convection.

is divided into six regions in the present study, i.e., $N = 6$. Thus six thermocouples are fixed at 33.5 mm in radius from the center of the circular tube and at $\pi/6$, $\pi/2$, $5\pi/6$, $7\pi/6$, $3\pi/2$ and $11\pi/6$ in angle, as shown in Fig. 2.

5. Results and discussion

The ratio of the surface area of the fin tip to the total fin surface area can be written as $\frac{R_o\delta}{(R_o^2-R_i^2)+R_o\delta}$. The "insulated tip" assumption in the present study will be reasonable provided that this ratio is very small. For simplicity, the average heat transfer coefficient on the tip surface can be assumed to be the same as that on the lateral surfaces of the fin. Based on experiment data of the present study, the surface area of the fin tip is only 2.14% of the total fin surface area. This implies that the assumption of Eq. (5) should be reasonable.

All the computations are performed with $N_r = 10$ and $N_\theta = 49$. The measured temperatures, T_1^{mea} $(33.5, \pi/6)$, T_2^{mea} $(33.5, \pi/2)$, T_3^{mea} $(33.5, 5\pi/6)$, $T_4^{mea}(33.5, 7\pi/6)$, T_5^{mea} $(33.5, 3\pi/2)$ and T_6^{mea} $(33.5, 11\pi/6)$, are respectively denoted as T_1^{mea}, T_2^{mea}, T_3^{mea}, T_4^{mea}, T_5^{mea} and T_6^{mea}. They are shown in Tables 1–3 for $V_{air} = 1$ m/s, 3 m/s and 5 m/s. $T_1^{mea} \neq T_6^{mea}$, $T_2^{mea} \neq T_5^{mea}$ and $T_3^{mea} \neq T_4^{mea}$ can be observed from Tables 1–3. This result shows further that the symmetric assumptions of the flow and thermal fields are not always very reasonable for the present problem. The similar phenomenon can also be found from Ref. [7]. Tables 1–3 also show the effect of the fin spacing S on the average heat transfer coefficient on the jth sub-fin region $\bar{h}_j$, heat transfer rate on the jth sub-fin region q_j, total heat transfer rate on the whole fin Q, average heat transfer coefficient $\bar{h}$ and fin efficiency η_f.

Due to the blockade of the tube, the airflow coming into the region between two parallel fins accelerates around a heated horizontal tube and forms a low-velocity wake region behind the tube. The boundary layer starts to develop at the front of the heated tube and increases in thickness along the circumference of this tube. Thus there exists a complex flow pattern within an annular-finned tube heat exchanger in forced convection. It can be found from Tables 1–3 that the measured fin temperatures on the downstream sub-fin regions 3 and 4 are higher than those on the other sub-fin regions for various V_{air} and S values. In addition, the average heat transfer coefficients on the downstream sub-fin regions 3 and 4 behind the tube are lower than those on the other sub-fin regions because these regions belong to the low-performance wake regions. Moreover, due to the formation of recirculating flow, the average heat transfer coefficients on the sub-fin regions 2 and 5, $\bar{h}_2$ and $\bar{h}_5$, can be larger than those on the downstream sub-fin regions 3 and 4, $\bar{h}_3$ and $\bar{h}_4$. It can be observed Tables 1–3 that $\bar{h}_2$ and $\bar{h}_5$ increase with increasing V_{air} for 1 m/s $\leqslant V_{air} \leqslant$ 5 m/s. The ratio of the $\bar{h}_2$ value for $V_{air} = 3$ m/s and 5 m/s to that for $V_{air} = 1$ m/s, respectively, is about 1.3 times and 2.8 times as $S = 0.005$ m. This implies that the horseshoe vortex effect can become more obvious with increasing the air velocity. The similar result can be found from Refs. [6,15]. The ratio of the average heat transfer coefficients on the front fin regions to those on the wake fin regions, $(\bar{h}_1 + \bar{h}_6)/(\bar{h}_3 + \bar{h}_4)$, respectively is about 6 times, 7 times and 6.5 times for $V_{air} = 1$ m/s, 3 m/s and 5 m/s as $S = 0.005$ m. This result shows that the heat transfer coefficient is much higher on the entrance fin region than on the wake fin region. The ratio of the heat transfer rates on the front fin regions to those on the wake fin regions, $(q_1 + q_6)/(q_3 + q_4)$, respectively is about 3.98 times, 4.27 times and 3.9 times for $V_{air} = 1$ m/s, 3 m/s and 5 m/s as $S = 0.005$ m. The results in Tables 1–3 also show that the heat transfer rate on the wake fin regions of the present finned-tube heat exchanger from $V_{air} = 1$ m/s to 5 m/s is responsible for 10.6–11.7% of the total heat transfer rate on the whole fin as $S = 0.005$ m

and for 14.7–20.9% as $S \geqslant 0.01$ m. The average heat transfer coefficient on each sub-fin region can be sensitive to the measured fin temperatures. However, the average heat transfer coefficient $\bar{h}$ seems to be not very sensitive to the measured fin temperatures for the present inverse scheme.

As stated by Hu and Jacobi [6], it was difficult to obtain fin efficiency measurements, because thermocouples on the fin surface can significantly alter the flow and heat transfer over the surface. This implies that the measured fin temperatures were inherently difficult to make without disrupting the heat transfer behavior. It can be observed from Tables 1–3 that the average heat transfer coefficient $\bar{h}$ increases with increasing the air speed V_{air} for 1 m/s $\leqslant V_{air} \leqslant$ 5 m/s ($1550 \leqslant Re_d \leqslant 7760$) and increasing the fin spacing S for 0.005 m $\leqslant S \leqslant$ 0.015 m. The $\bar{h}$ value in the range of $V_{air} = 1$ m/s to 5 m/s increases from 24.63 W/m^2 K to 76.92 W/m^2 K for $S = 0.005$ m and from 28.42 W/m^2 K to 87.30 W/m^2 K for $S = 0.015$ m. The fin efficiency η_f decreases with increasing V_{air} for 1 m/s $\leqslant V_{air} \leqslant$ 5 m/s and seems to be not very sensitive to the fin spacing. The η_f value in the range of $V_{air} = 1$ m/s to 5 m/s decreases from 0.38 to 0.25 for $S = 0.005$ m and from 0.36 to 0.24 for $S = 0.015$ m. It can be observed that the present estimates of the η_f value are higher than those obtained from a vertical square fin [7]. Fig. 5 shows variation of the $\bar{h}$ value with S/h_f for various Re_d values, where h_f denotes the fin height and is equal to 36 mm in the present study. It can be found from Fig. 5 that the $\bar{h}$ value approaches the asymptotical value obtained from a single annular circular fin as $S \to \infty$. The effect of the fin spacing S on the $\bar{h}$ value can be negligible when the S/h_f value exceeds about 0.5. The similar phenomenon can also be observed from Ref. [7].

Based on Eqs. (14) and (17), the present estimate of the average heat transfer coefficient under the ideal isothermal condition $\bar{h}^{iso}$ can be determined from the following expression:

$$Q = \sum_{j=1}^{N} 2\bar{h}_j \int_{A_j} (T - T_\infty) \mathrm{d}A = 2\bar{h}^{iso} A_f (T_o - T_\infty) \tag{20}$$

In order to validate the reliability of the present inverse scheme, Tables 1–4, respectively, show comparisons between the present estimates of the $\bar{h}^{iso}$ value and those given by Hu and Jacobi [6] and Watel et al. [14].

It can be found from Ref. [14] that the correlated relationship of Nu_d^{iso} and Re_d for $2550 \leqslant Re_d \leqslant 42000$ and various fin spacings was expressed as

$$Nu_d^{iso} = 0.446 \left[\left(\frac{\delta}{S} + 1 \right) \left(1 - \frac{K^*}{(S/d_o)^b (Re_d)^{0.07}} \right) \right]^{0.55} Re_d^{0.55} \tag{21}$$

where all the properties are evaluated at the film temperature T_f. Re_d and Nu_d^{iso} are respectively denoted as the Reynolds number based on the outer diameter of the circular tube and the Nusselt number based on the temperature difference of T_o and T_∞. Nu_d^{iso} and Re_d are defined as

$$Nu_d^{iso} = \frac{\bar{h}_d^{iso} d_o}{k_{air}} \tag{22}$$

and

$$Re_d = \frac{V_{air} d_o}{v} \tag{23}$$

where k_{air} is the thermal conductivity of the air v is the kinematic viscosity.

The parameters b and K^* are given as

$$b = 0.27, \quad K^* = 0.62 \quad \text{for } 0.034 \leqslant S/d_o \leqslant 0.14$$

and

$$b = 0.55, \quad K^* = 0.36 \quad \text{for } 0.14 \leqslant S/d_o$$

In order to compare with the estimated results given by Hu and Jacobi [6], the Reynolds number based on the hydraulic diameter of the heat exchanger Re is introduced as

$$Re_d = \frac{V_{max} D_H}{v} \tag{24}$$

where V_{max} is the maximum flow speed at the minimum flow area. D_H is the hydraulic diameter of the heat exchanger.

In order to match the present estimates of Nu_d^{iso} and η_f for various Re_d, S and d_o values, the modification of Eq. (21) in conjunction with the present estimates and the predicted results given by Hu and Jacobi [6] can yield the correlation of Nu_d^{iso}, Re_d, d_o and S as

$$Nu_d^{iso} = 16.5185 d_o \left[\left(2.54 \frac{\delta}{S} + 0.6925 \right) Re_d \times \left(1 - \frac{K^*}{(S/d_o)^b (Re_d)^{0.07}} \right) \right]^{0.55} \left(\frac{1}{V_{air}} \right)^{0.123} \tag{25}$$

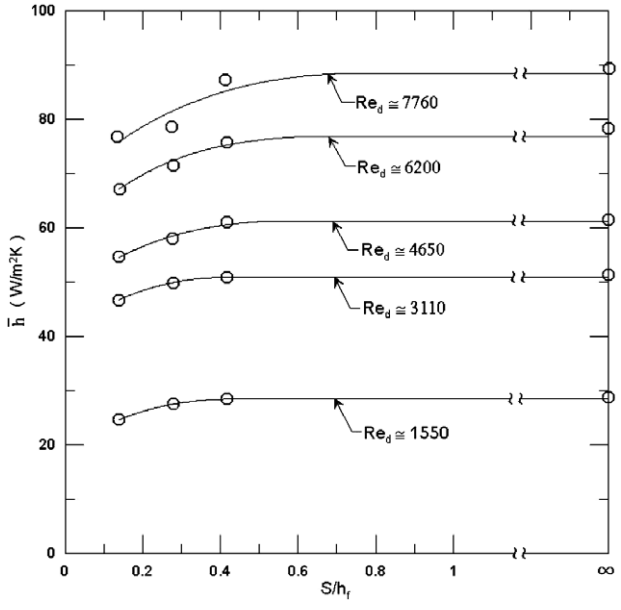

Fig. 5. Variation of the $\bar{h}$ value with S/h_f for various Re_d values.

Table 4
Comparison of the $\bar{h}^{iso}$ value between the present estimates and previous results for various V_{air} or Re values

			$\bar{h}^{iso}$W/(m^{2}K)				
			$S = 0.005$ m	$S = 0.0061$ m	$S = 0.01$ m	$S = 0.015$ mm	S → ∞
$V_{air} = 2$ m/s	Present	Eq. (20)	26.93	–	29.36	29.53	29.81
		Eq. (25)	25.64	–	26.42	26.56	28.27
	Ref. [14]		27.92	–	31.82	32.53	37.68
$V_{air} = 4$ m/s	Present	Eq. (20)	34.45	–	36.76	38.31	39.40
		Eq. (25)	35.40	–	36.00	36.07	38.03
	Ref. [14]		41.98	–	46.37	48.10	55.18
$Re = 3320$	Present Eq. (25)		–	33.91	–	–	–
	Ref. [6]		–	31.6	–	–	–
$Re = 5980$	Present Eq. (25)		–	44.7	–	–	–
	Ref. [6]		–	45.5	–	–	–
$Re = 6880$	Present Eq. (25)		–	47.70	–	–	–
	Ref. [6]		–	49.5	–	–	–
$Re = 7580$	Present Eq. (25)		–	49.94	–	–	–
	Ref. [6]		–	50.5	–	–	–
$Re = 8440$	Present Eq. (25)		–	52.5	–	–	–
	Ref. [6]		–	55.8	–	–	–

The correlation of η_f, Re_d, d_o and S for the present estimates can be expressed as

$$\eta_f = \left(0.208\frac{\delta}{S} + 1\right)[0.40783 - 4.17947 \times 10^{-5} Re_d + 2.598 \times 10^{-9}(Re_d)^2]\left(1 + \frac{25.61}{(S/d_o)^{0.55} Re_d}\right) \quad (26)$$

It can be found from Ref. [16] that the correlated relationship of Nu_d^{iso} and Re_m for $S_T/(2R_o) \leqslant 1.52$ and $(2R_o)/d_o = 1.8$ was expressed as

$$Nu_d^{iso} = 0.0529 Re_m^{0.704} \quad (27)$$

where all the properties are also evaluated at the film temperature T_f. The parameter S_T denotes the transverse pitch between two neighboring tube centers. Re_m is the Reynolds number and is defined as

$$Re_m = \frac{V_{max} d_o}{v} \quad (28)$$

In Eq. (28), V_{max} is the maximum flow speed at the minimum flow area.

Comparisons of $\bar{h}^{iso}$ between the present estimates obtained from Eqs. (20) and (25) and those given by Watel et al. [14] are shown in Tables 1–4 for various S values and 1 m/s $\leqslant V_{air} \leqslant$ 5 m/s. It is found from Table 1 that the present estimates of the $\bar{h}^{iso}$ value are in good agreement with those given by Watel et al. [14] for 0.005 m $\leqslant S \leqslant$ 0.015 m and $V_{air} = 1$ m/s. However, inspection of Tables 1–4 reveals that the present estimates of the $\bar{h}^{iso}$ value for $V_{air} = 1$ m/s and $S \to \infty$ and for $V_{air} \geqslant 2$ m/s are lower than those given by Watel et al. [14]. This deviation seems to become large with increasing V_{air} or S. It may result from measurement locations and some experimental uncertainties such as personal fluctuations, circumstance of the experiment and experimental measurements, etc. It is found from Ref. [14] that the measurement of the flow velocity and a thermocouple, respectively, was located at the wind tunnel section 280 mm and 80 mm upstream the fins. Obviously, these two measurement locations are different from the present measurement locations.

Comparisons of the $\bar{h}^{iso}$ value between the present estimates obtained from Eq. (25) and those given by Hu and Jacobi [6] are also shown in Table 4 for $S = 0.0061$ m, $d_o = 0.0381$ m, $\delta = 0.00102$ m, $T_o = 80.2$ °C, $T_\infty = 27$ °C and various Re values. Maybe, due to the inattention of the authors, their estimated results for $Re = 5980$ and 6880 can be in error, as shown in Table 2 of Ref. [6]. It can be observed from Tables 1–4 that the $\bar{h}^{iso}$ values obtained from the present correlation of Nu_d^{iso} shown in Eq. (25) agree with those obtained from Eq. (20). Of the 25 data used to develop this correlation, 22 fall about within ±6% of the values obtained from Eq. (25). Table 4 also shows that the present estimates of the $\bar{h}^{iso}$ values obtained from Eq. (25) agree with those given by Hu and Jacobi [6] for $3320 \leqslant Re \leqslant 8440$ ($5920 \leqslant Re_d \leqslant 15050$). This implies that the present inverse scheme should have good reliability and good accuracy for the present problem. Saboya and Sabora [22] have ever stated that the naphthalene vapor concentration at the subliming wall was very sensitive to the wall temperature, which was practically equal to the ambient temperature. In order to minimize experimental errors in the determination of the Sherwood numbers, the laboratory room was temperature controlled.

Once the average heat transfer coefficient on each sub-fin region is obtained, the temperature distribution on the fin can also be determined from Eq. (13). Because the average heat transfer coefficient on each sub-fin region is the approximate value, the temperature distribution on the fin is an approximate contour for various V_{air} and S values.

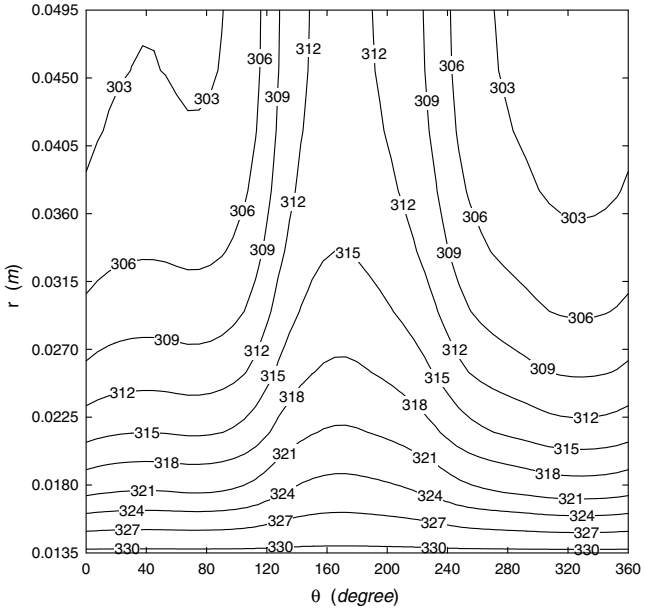

Fig. 6. Distribution of the calculated fin temperature for $S = 0.005$ m and $V_{air} = 1$ m/s.

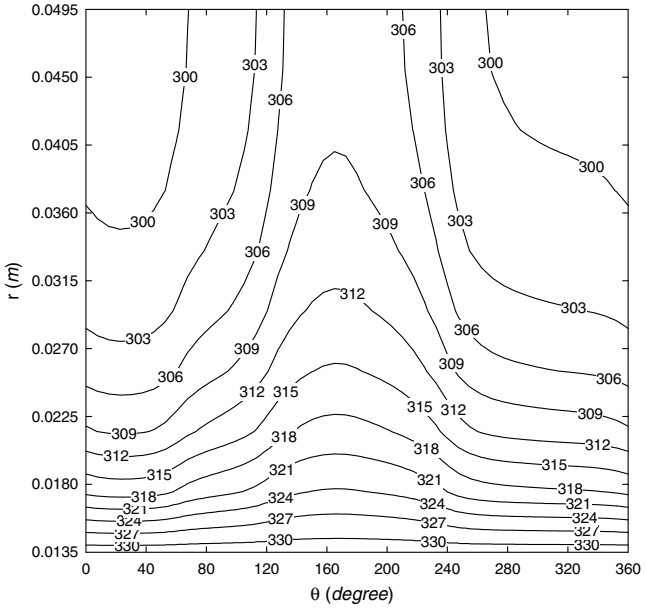

Fig. 7. Distribution of the calculated fin temperature for $S = 0.005$ m and $V_{air} = 3$ m/s.

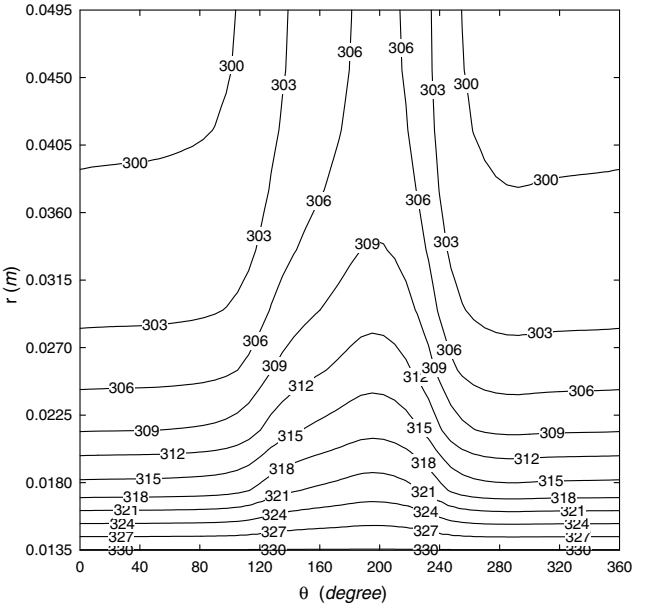

Fig. 8. Distribution of the calculated fin temperature for $S = 0.005$ m and $V_{air} = 5$ m/s.

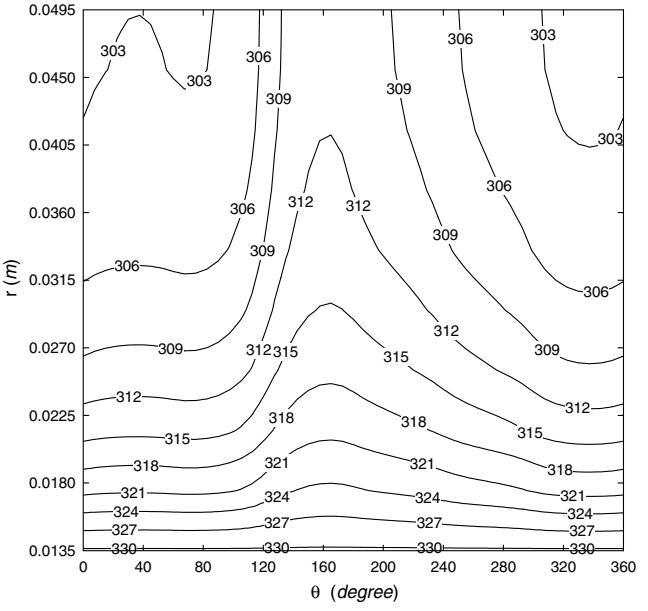

Fig. 9. Distribution of the calculated fin temperature for $S = 0.015$ m and $V_{air} = 1$ m/s.

Figs. 6–8, respectively, show the distributions of the calculated temperature on the fin for $V_{air} = 1$ m/s, 3 m/s and 5 m/s as $S = 0.005$ m. The distributions of the calculated fin temperature for $V_{air} = 1$ m/s, 3 m/s and 5 m/s are, respectively, shown in Figs. 9–11 as $S = 0.015$ m. It can be observed from Figs. 6–11 that, due to the poor thermal conductivity of the stainless fin, there is a considerable temperature drop between the tube wall and the edge of the fin especially on the upstream region. The fin temperature distributions obviously depart from the ideal isothermal situation and the fin temperature decreases more rapidly away from the circular center when V_{air} increases. Due to the above phenomenon, the fin efficiency decreases with increasing the frontal air speed or the Reynolds number.

6. Conclusions

The present study proposes a numerical inverse scheme involving the finite difference method in conjunction with the least-squares method and experimental fin tempera-

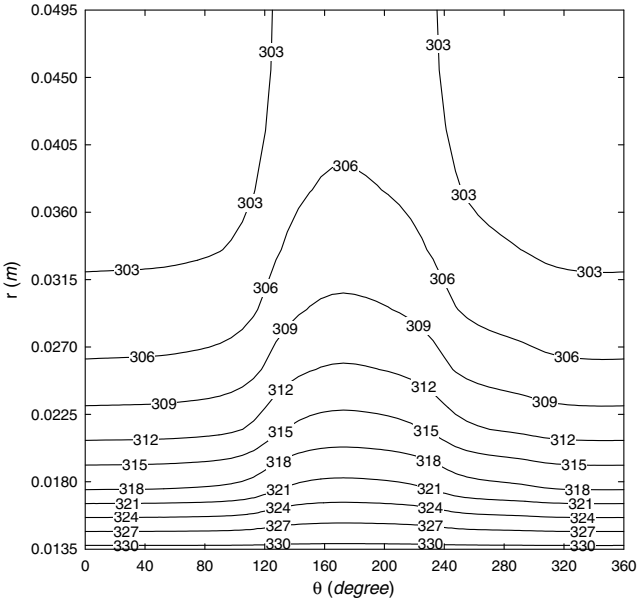

Fig. 10. Distribution of the calculated fin temperature for $S = 0.015$ m and $V_{air} = 3$ m/s.

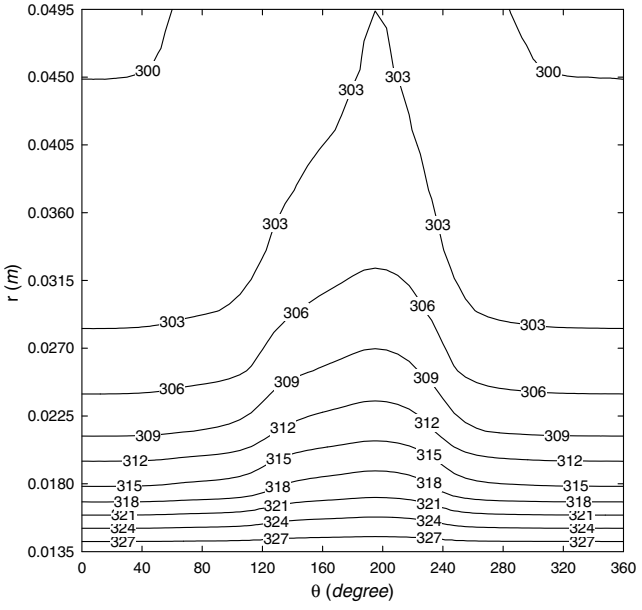

Fig. 11. Distribution of the calculated fin temperature for $S = 0.015$ m and $V_{air} = 5$ m/s.

tures to estimate the unknown heat transfer coefficients on sub-fin regions, average heat transfer coefficient on the whole fin $\bar{h}$ and fin efficiency η_f for various V_{air} and S values. The estimated results show that there is a considerable temperature drop between the tube wall and the edge of the annular circular fin especially on the upstream region. The fin temperature distributions depart from the ideal isothermal situation and the fin temperature decreases more rapidly away from the circular center with increasing the air speed. The ratio of the average heat transfer coefficient on the front fin region to that on the wake fin region can be up to seven times for a given V_{air} value. The $\bar{h}$ value increases with increasing V_{air} for $1\ \text{m/s} \leqslant V_{air} \leqslant 5\ \text{m/s}$ and increasing S for $0.005\ \text{m} \leqslant S \leqslant 0.018\ \text{m}$. However, the effect of the fin spacing S on the $\bar{h}$ value can be negligible when the S value exceeds about 0.018 m. The η_f value decreases with increasing V_{air} for $1\ \text{m/s} \leqslant V_{air} \leqslant 5\ \text{m/s}$ and seems to be not very sensitive to the fin spacing. An important finding is that the present estimated results can be applied to obtain the new correlations of the Nusselt number and fin efficiency based on d_o, S and Re_d. The present estimates obtained from the correlation of the Nusselt number agree with those given by Hu and Jacobi [6] for $3320 \leqslant Re \leqslant 8440$. This implies that the present inverse scheme should have good reliability and good accuracy.

Acknowledgement

The authors gratefully acknowledge the financial support provided by the National Science Council of the Republic of China under Grant No. NSC 92-2622-E006-146.

References

[1] G.D. Raithby, K.G.T. Hollands, Natural convection, in: W.M. Rohsenow, J.P. Hartnett, E.N. Ganic (Eds.), Handbook of Heat Transfer Fundamentals, second ed., McGraw-Hill, New York, 1985.
[2] J.L. Lage, Tube-to-tube heat transfer degradation effect on finned-tube heat exchangers, Numer. Heat Transfer A 39 (2001) 321–337.
[3] H.J. Sung, J.S. Yang, T.S. Park, Local convective mass transfer on circular cylinder with transverse annular fins in crossflow, Int. J. Heat Mass Transfer 39 (1996) 1093–1101.
[4] T.W.H. Sheui, S.F. Tsai, T.P. Chiang, Numerical study of heat transfer in two-row heat exchangers having extended fin surfaces, Numer. Heat Transfer A 35 (1999) 797–814.
[5] M. Tutar, A. Akkoca, Numerical analysis of fluid flow and heat transfer characteristics in three-dimensional plate fin-and-tube heat exchangers, Numer. Heat Transfer A 46 (2004) 301–321.
[6] X. Hu, A.M. Jacobi, Local heat transfer behavior and its impact on a single-row, annularly finned tube heat exchanger, ASME J. Heat Transfer 115 (1993) 66–74.
[7] H.T. Chen, J.C. Chou, H.C. Wang, Estimation of heat transfer coefficient on a vertical plate fin of finned-tube heat exchangers for various air speeds and fin spacings, Int. J. Heat Mass Transfer 50 (2007) 45–57.
[8] R.L. Webb, Principles of Enhanced Heat Transfer, Wiley, New York, 1994, pp. 125–153.
[9] Ş. Yildiz, H. Yüncü, An experimental investigation on performance of annular fins on a horizontal cylinder in free convection heat transfer, Heat Mass Transfer 40 (2004) 239–251.
[10] Y.A. Çengel, Heat Transfer – A Practical Approach, second ed., McGraw-Hill, New York, 2004, pp. 486–488.
[11] M.N. Özisik, Heat Conduction, second ed., Wiley, New York, 1993 (Chapter 14).
[12] K. Kurpisz, A.J. Nowak, Inverse Thermal Problems, Computational Mechanics Publications, Southampton, UK, 1995.
[13] H.T. Chen, W.L. Hsu, Estimation of heat transfer coefficient on the fin of annular finned-tube heat exchangers in natural convection for various fin spacings, Int. J. Heat Mass Transfer 50 (2007) 1750–1761.
[14] B. Watel, S. Harmand, B. Desmet, Influence of flow velocity and fin spacing on the forced convective heat transfer from an annular-finned tube, JSME Int. J., Ser. B 42 (1) (1999) 56–64.
[15] M.S. Mon, U. Gross, Numerical study of fin-spacing effects in annular-finned tube heat exchangers, Int. J. Heat Mass Transfer 47 (2004) 1953–1964.

[16] E.M. Sparrow, F. Samie, Heat transfer and pressure drop results for one-and two-row arrays of finned tubes, Int. J. Heat Mass Transfer 28 (1985) 2247–2259.
[17] R.S. Matos, J.V.C. Vargas, T.A. Laursen, A. Bejan, Optimally staggered finned circular and elliptic tubes in forced convection, Int. J. Heat Mass Transfer 47 (2004) 1347–1359.
[18] J.Y. Jang, The development of high efficiency air-cooled steam condenser for the power plant, Report of National Council Science, NSC 92-2622-E006-146, Taiwan, 2004.
[19] F. Kreith, M.S. Bohn, Principles of Heat Transfer, fifth ed., West Publishing Co., New York, 1993.
[20] A. Bejan, Heat Transfer, John Wiley and Sons Inc., New York, 1993, pp. 53–62.
[21] V.S. Arpaci, S.H. Kao, A. Selamet, Introduction to Heat Transfer, Prentice-Hall, NJ, 1999, pp. 202–205.
[22] S.M. Saboya, F.E.M. Saboya, Experimental on elliptic sections in one- and two-row arrangements of plate fin and tube heat exchangers, Exp. Therm. Fluid Sci. 24 (2001) 67–75.